

# Quantum Gravitational Sensor for Space Debris

Meng-Zhi Wu,<sup>1</sup> Marko Toroš,<sup>2</sup> Sougato Bose,<sup>3</sup> and Anupam Mazumdar<sup>1</sup>

<sup>1</sup>*Van Swinderen Institute, University of Groningen, 9747 AG, The Netherlands*

<sup>2</sup>*School of Physics and Astronomy, University of Glasgow, Glasgow, G12 8QQ, UK*

<sup>3</sup>*Department of Physics and Astronomy, University College London,  
Gower Street, WC1E 6BT London, United Kingdom*

Matter-wave interferometers have fundamental applications for gravity experiments such as testing the equivalence principle and the quantum nature of gravity. In addition, matter-wave interferometers can be used as quantum sensors to measure the local gravitational acceleration caused by external massive moving objects, thus lending itself for technological applications. In this paper, we will establish a three dimensional model to describe the gravity gradient signal from an external moving object, and theoretically investigate the achievable sensitivities using the matter-wave interferometer based on the Stern-Gerlach set-up. As an application we will consider the Mesoscopic Interference for Metric and Curvature (MIMAC) and Gravitational wave detection scheme [New J. Phys. 22, 083012 (2020)] and quantify its sensitivity to gravity gradients using frequency-space analysis. We will consider objects near Earth-based experiments and space debris in proximity of satellites and estimate the minimum detectable mass of the object as a function of their distance, velocity, and orientation. We will conclude by estimating the requirements to sense gravity gradients from asteroids, planetary motion and from outer solar system primordial black holes.

## 1. INTRODUCTION

Interferometry has many salient applications [1] in gravity experiments such as testing the equivalence principle [2–4] and measuring the Earth’s gravitational acceleration [5–14]. The seminal works on neutron interferometry [15–17] motivated a series of matter-wave interferometers [18–21] as well as led to more recent developments in photon interferometry [22–27].

One of the latest quests is to build a matter-wave interferometer with nanoparticles to test the quantum nature of gravity in a laboratory [28, 29] (for a related work see [30]). The scheme relies on two masses, each prepared in a spatial superposition, and placed at distances where they couple gravitationally, but still sufficiently far apart that all other interactions remain suppressed. If gravity is a bonafide quantum entity, and not a classical real-valued field, then the two masses will entangle [31–34]. To test the quantum nature of gravity we will need particles of mass  $\sim 10^{-14} - 10^{-15}$  kg, an interferometric scheme for preparing large superposition sizes  $\sim 100 \mu\text{m}$ , and exquisite experimental control to guarantee coherence times of  $\sim 1$  s [28, 35–41].

One of the most promising approaches towards interferometry with nanoparticles is based on the Stern-Gerlach (SG) apparatus [42]. SG interferometers have been already experimentally realized using an atom chip [43], with the half-loop [44] and full-loop [45] configurations achieving the superposition size of  $3.93 \mu\text{m}$  and  $0.38 \mu\text{m}$  in the experimental time of 21.45 ms and 7 ms, respectively [45]. This basic SG scheme can be adapted to the mass range of nanoparticles using nanodiamond like materials with embedded nitrogen vacancy (NV) centers. Such a system has an internal spin degree of freedom and can thus be placed in a large spatial superposition using the SG setup [28, 46–49].

One of the main challenges of nanocrystal matter-

wave interferometry is to tame the numerous decoherence and noise sources. Common sources for the loss of visibility, such as the ones arising from residual gas collisions and environmental photons, can be attenuated by vacuum and low-temperature technologies [35–41]. In addition, the spin decoherence should also be taken into account, i.e., the Humpty-Dumpty effect [47, 50–53], with methods to extend the spin coherence time, as well as tackle the Majorana spin-flip, under development [46, 47, 54]. Moreover, there are also a series of gravitational channels for decoherence; the emission of gravitons is negligible [55], decoherence induced by the gravitational interaction with the experimental apparatus can be reduced using a hierarchy of distances [56], and gravity gradient noise (GGN) can be mitigated with an exclusion zone [37]. GGN is equally important for the gravitational wave observatories [57] such as LIGO [58, 59], Virgo [60, 61], KAGRA [62] and the Einstein Telescope [63], in particular at the low frequencies.

In this work, we will investigate the possibility of using the nanoparticle matter-wave interferometer as a *GGN quantum sensor*. We will estimate the required sensitivities to detect the motion of external objects flying at small and large impact parameters and with varying velocities. Such a device can be regarded as a quantum version of accelerometers, gravimeters and gradiometers [64–68].

We will first make a brief review about sensing with matter-wave interferometers in the language of Feynman’s path integral approach (Sec. 2). As will be shown, the phase fluctuation density in the frequency space can be factorized into a noise part (described by the corresponding power spectrum density) multiplied by the trajectory part (described by the so-called transfer function). Then, we will establish a three dimensional model for the GGN caused by external objects, in particular, ob-

taining the relation between local acceleration noise and phase fluctuation (Sec. 4), and show that it reduces to the two-dimensional model from [69] (see Appendix B). We will apply the model to evaluate the possibility of tracking slow moving matter in Earth-based laboratories and space debris in the proximity of satellites using the Mesoscopic Interference for Metric and Curvature (MIMAC) and Gravitational wave interferometer [6] (Sec. 5.1), and give a comparison to the Quantum Gravity Entanglement of Masses (QGEM) dual interferometer [28, 29, 37] (see Appendix B). We will conclude by estimating the interferometric requirements for probing the GGN generated by planetary motion and outer solar system black holes (Sec. 5.2).

## 2. NOISES IN THE MATTER-WAVE INTERFEROMETRY

In this section, we will give a brief pedagogical introduction to the matter-wave sensing with nanoparticles. According to Feynman's path integral method, the quantum phase along each path can be obtained from the action, and the signal in the experiment is described by the phase difference [70]:

$$\begin{aligned}\phi_0 &= \phi_R - \phi_L \\ &= \frac{1}{\hbar} \int_{t_i}^{t_f} L_R[x_R, \dot{x}_R] - L_L[x_L, \dot{x}_L] dt,\end{aligned}\quad (1)$$

where  $t_i$  and  $t_f$  are the time of splitting and recombination of the two beams,  $L_{L,R}$  is the Lagrangian of the left and right arm which is a functional of the coordinate  $x_{L,R} \equiv x_{L,R}(t)$  and the velocity  $\dot{x}_{L,R} \equiv \dot{x}_{L,R}(t)$ . Supposing that the Lagrangian can be expanded as a Taylor series in  $x_{L,R}$ , and that the noises can be described as the fluctuation of the coefficients, we find:

$$\begin{aligned}L_{L,R}[x_{L,R}, \dot{x}_{L,R}] &= \frac{1}{2} m \dot{x}_{L,R}^2 \\ &\quad - m a_{0;L,R} x_{L,R} - \frac{1}{2} m \omega_{0;L,R}^2 x_{L,R}^2 \\ &\quad - m a_{\text{noise}} x_{L,R} - \frac{1}{2} m \omega_{\text{noise}}^2 x_{L,R}^2 \\ &\quad + \mathcal{O}(x_{L,R}^3),\end{aligned}\quad (2)$$

where  $m$  is the mass of the interferometer,  $a_{0;L,R}$  and  $\omega_{0;L,R}^2$  are controlled by the experiment, and  $a_{\text{noise}} \equiv a_{\text{noise}}(t)$  and  $\omega_{\text{noise}}^2 \equiv \omega_{\text{noise}}^2(t)$  are time-varying stochastic quantities. In particular, the GGN will be described by the quadratic term, so we will focus on  $\omega_{\text{noise}}^2$  in the rest of this section. In principle,  $a_{\text{noise}}$  and noises coupling higher order terms  $\mathcal{O}(x_{L,R}^3)$  can be studied in the same way. Since the noise can be modelled as a fluctuation in the Lagrangian, it will contribute to a fluctuation in the phase difference  $\phi_0 = \phi_R - \phi_L$ , given by

$$\delta\phi_0 = \frac{m}{2\hbar} \int_{t_i}^{t_f} \omega_{\text{noise}}^2 (x_R^2 - x_L^2) dt.\quad (3)$$

Experimentally measurable statistical quantities are obtained by taking the average value  $\mathbb{E}[\cdot]$ <sup>1</sup>. The mean value of the noise  $\mathbb{E}[\omega_{\text{noise}}^2(t)]$  can be assumed to be zero by adding an offset on the baseline of the signal in experiments<sup>2</sup>. The autocorrelation function  $\mathbb{E}[\omega_{\text{noise}}^2(t_1)\omega_{\text{noise}}^2(t_2)]$  can be related to the Fourier transformation of the corresponding power spectrum density (PSD) of the noise, denoted as  $S_{\text{noise}}(\omega, t)$ , using the Wiener-Khinchin theorem. We further suppose the noise is stationary (i.e., its properties do not change over time), such that the PSD becomes time-independent  $S_{\text{noise}}(\omega, t) = S_{\text{noise}}(\omega)$  (see for example [72]).

Summarizing, the noise  $\omega_{\text{noise}}^2(t)$  is characterized by the following statistical quantities:

$$\begin{aligned}\mathbb{E}[\omega_{\text{noise}}^2(t)] &= 0, \\ \mathbb{E}[\omega_{\text{noise}}^2(t_1)\omega_{\text{noise}}^2(t_2)] &= \frac{1}{2\pi} \int_{\omega_{\min}}^{\infty} S_{\text{noise}}(\omega) e^{i\omega(t_1-t_2)} d\omega.\end{aligned}\quad (4)$$

The lower bound of the integral  $\omega_{\min}$  is determined by the total experiment time  $t_{\text{exp}} = t_f - t_i$ , i.e.  $\omega_{\min} = 2\pi/t_{\text{exp}}$  according to the finite Fourier transformation.

Using Eqs. (3) and (4), we find that the average value of the phase fluctuation vanishes, while the variance is given by

$$\Gamma_{\text{noise}} \equiv \mathbb{E}[(\delta\phi_0)^2] = \frac{1}{2\pi} \left(\frac{m_0}{2\hbar}\right)^2 \int_{\omega_{\min}}^{\infty} S_{\text{noise}}(\omega) F(\omega) d\omega,\quad (5)$$

where  $F(\omega)$  is defined by

$$\begin{aligned}F(\omega) &= \int dt_1 \int dt_2 (x_R^2(t_2) - x_L^2(t_2)) \\ &\quad (x_R^2(t_1) - x_L^2(t_1)) e^{i\omega(t_1-t_2)}.\end{aligned}\quad (6)$$

Since  $F(\omega)$  only depends on the trajectories of the two arms, we will call it the *transfer function* of the interferometer [73], which means it transfers the PSD of the noise into the phase fluctuation of the interferometer. Mathematically, the transfer function  $F(\omega)$  can be

<sup>1</sup> The symbol  $\mathbb{E}[\cdot]$  represents the statistical average of a stochastic quantity, i.e., the average over different realizations of the noise. However, for a time-varying ergodic noise, the averaging can be also performed in time using a single realization of the noise. For example, the average of a time-varying stochastic quantity  $\delta\phi(t)$  can be formulated as

$$\mathbb{E}[\delta\phi] = \frac{1}{T} \int_0^T \delta\phi(t) dt,$$

where  $T$  should be much longer than any time scale characterizing the statistical properties of the noise. More pedagogic materials can be found in [71].

<sup>2</sup> The baseline (i.e., the zero-point) of the phase has to be calibrated before the experiment starts, so the contribution of the mean value of every noise will be taken into account in the offset of the baseline. Therefore, the mean value of a noise  $\mathbb{E}[\omega_{\text{noise}}^2(t)]$  can be always assumed to be zero.

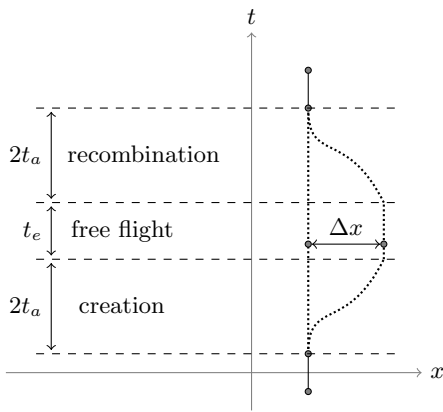


FIG. 1: Illustration of the paths of the two arms of the interferometer. The acceleration direction of the right arm is along "+" direction of the x-axis during the time range  $[0, t_a]$  and  $[3t_a + t_e, 4t_a + t_e]$ , while it is along "-" direction during  $[t_a, 2t_a]$  and  $[2t_a + t_e, 3t_a + t_e]$ . In the interval  $[2t_a, 2t_a + t_e]$  the right paths follow geodesic motion, while the motion of the left arm is purely geodesic. A single interferometer must be asymmetric to be sensitive to GGN as one can always choose the origin of the harmonic trap generated by the GGN to be at the center of the two paths (a single symmetric interferometer would thus acquire only a global phase from any harmonic perturbation as the two paths would acquire exactly the same phase). We also assume that the setup is freely falling under gravity.

simplified into several equivalent expressions <sup>3</sup>

$$F(\omega) = \left| \int e^{i\omega t} (x_R^2(t) - x_L^2(t)) dt \right|^2$$

$$= \frac{1}{\omega^2} \left| \int e^{i\omega t} \frac{d}{dt} (x_R^2(t) - x_L^2(t)) dt \right|^2. \quad (7)$$

According to expression Eq.(7), the transfer function  $F(\omega)$  is the modulus square of a complex number integration, so it is always a real valued function. In the low-frequency regime,  $\omega \ll 2\pi/t_{\text{exp}}$  (although this region is negligible according to the lower bound of the finite Fourier transformation), the factor  $e^{i\omega t}$  in the first expression approximately equals one, then  $F(\omega)$  approximately equals  $(\int (x_R^2(t) - x_L^2(t)) dt)^2$ , which is independent of the frequency  $\omega$ .

For the high-frequency noises,  $F(\omega)$  decreases as  $\omega^{-2}$ , according to the second expression. Therefore, the transfer function  $F(\omega)$  can suppress the high-frequency noises. In addition, the total phase fluctuation,  $\Gamma_{\text{noise}}$ , is sensitive to the lower bound  $\omega_{\text{min}} = 2\pi/t_{\text{exp}}$  of the integration, see Eq.(5). In particular, for a shorter experimental time

$t_{\text{exp}}$ , larger is the integral bound  $\omega_{\text{min}}$ , and hence smaller will be the total phase fluctuation,  $\Gamma_{\text{noise}}$ .

We consider the specific configuration shown in Fig. 1 [6]. The interferometer is set to freely fall, and the creation and recombination stages control the superposition along the x-axis. For simplicity, the acceleration during the splitting and recombining parts is assumed to be constant, which can be achieved in a Stern-Gerlach apparatus with constant magnetic field gradient. The absolute value of the acceleration is given by

$$a_m = \frac{g\mu_B}{m_0} |\nabla B|, \quad (8)$$

where  $g = 2$  is the Lande g-factor,  $\mu_B = 9 \times 10^{-24}$  J/T is the Bohr magneton,  $m_0$  is the mass of the interferometer and  $\nabla B = 10^4$  T/m is the gradient of the magnetic field. The direction of the acceleration  $a_m$  depends on both the gradient of the magnetic field and the value of the spin in each arm. The magnetic field gradient makes the system on the right path accelerate during  $[0, t_a]$  and  $[2t_a + t_e, 3t_a + t_e]$ , decelerate during  $[t_a, 2t_a]$  and  $[3t_a + t_e, 4t_a + t_e]$ , while in the intermediate interval  $[2t_a, 2t_a + t_e]$  it is vanishingly small, while the part of the system on the left path is in free-fall. The transfer function for such an interferometer is given by <sup>4</sup>:

$$F(\omega) = 16 \frac{a_m^4}{\omega^{10}} \left( -t_a^2 \omega^2 \sin(\omega(t_a + t_e/2)) \right. \\ \left. + (t_a^2 \omega^2 + 3) \sin(t_e \omega/2) - 3 \sin(\omega(2t_a + t_e/2)) \right. \\ \left. + 6t_a \omega \cos(\omega(t_a + t_e/2)) \right)^2. \quad (9)$$

We note that Eq. (9) is the transfer function for the MI-MAC scheme discussed in [6] and can be used to carry out frequency-space noise analysis of any type. The transfer function  $F(\omega)$  is plotted in Fig. 2 with different values for the splitting time  $t_a$ , the free-falling time  $t_e$ , and the interferometer mass  $m_0$ .

As shown in sub-figures (a) and (b) of Fig. 2, the splitting time,  $t_a$ , and the free-falling time,  $t_e$ , significantly affect on the behaviour of the transfer function  $F(\omega)$ . The splitting time has a greater impact on the absolute value of  $F(\omega)$ , while the free-falling time has a greater impact on the oscillatory behaviour of  $F(\omega)$ .

At low frequency,  $\omega \ll 2\pi/(4t_a + t_e)$ , we find that  $F(\omega)$  reaches the constant value <sup>5</sup>  $\Delta x^4 (23t_a + 15t_e)^2 / 225$ , which

<sup>3</sup> The variables  $t_1$  and  $t_2$  of the double integral Eq.(6) can be separated, then this integral is transformed into the product of two single-variable integrals, i.e., the first line in Eq.(7), and the second line in Eq.(7) can be obtained via integration by parts.

<sup>4</sup> A similar form of the transfer function has been obtained also in [37] for two case of two symmetric interferometers located at distance  $\pm d/2$  from the origin (i.e., a dual two-particle interferometer). Each interferometer is located asymmetrically with respect to the origin (i.e., either left or right of the origin). As the origin coincides with center of the harmonic GGN trap, each individual interferometer acquired different GGN phases on the two arms, leading to a GGN signature in the combined dual two-particle interferometer. For more details see Appendix B.

<sup>5</sup> Using  $\sin u \approx u$  for  $u \ll 1$  in Eq.(9) and introducing  $\Delta x = a_m t_a^2$ .

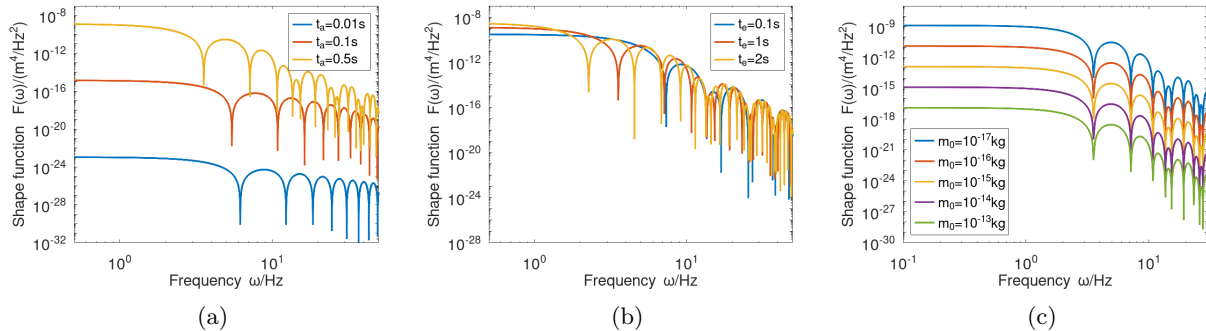


FIG. 2: The transfer function for the asymmetric interferometer configuration for different experimental parameters. The fixed parameters is  $\nabla B = 10^4$  T/m (i.e.  $a_m = 1.8 \times 10^{-2}$  m/s<sup>2</sup>) in all the figures. We set the other parameters to:  $m_0 = 10^{-17}$  kg and  $t_e = 1$  s in the sub-figure (a),  $m_0 = 10^{-17}$  kg and  $t_a = 0.5$  s in the sub-figure (b), and  $t_a = 0.5$  s and  $t_e = 1$  s in the sub-figure (c). The transfer function  $F(\omega)$  approaches a constant value in the low-frequency range. By comparing the sub-figures (a) with (b), we find that the transfer function  $F(\omega)$  is more sensitive to the value of the splitting time  $t_a$ , than the free-falling time  $t_e$ , especially in the low-frequency range. As can be seen from the sub-figure (c), the transfer function  $F(\omega)$  is inversely proportional to the mass square  $m_0^2$  of the interferometer. Hence the phase fluctuation  $\Gamma_{\text{noise}}$  in Eq.(5) is independent of the mass of the interferometer.

is much more sensitive to the value of  $t_a$  than to the value of  $t_e$ . Setting  $t_e = 0$ , we find a simple formula for the transfer function in the low frequency regime:

$$\bar{F} \equiv \lim_{\omega \rightarrow 0} F(\omega) = \frac{529}{225} \Delta x^4 t_a^2. \quad (10)$$

In the high-frequency region,  $\omega \gg 2\pi/(4t_a + t_e)$ , the transfer function  $F(\omega)$  decreases rapidly as  $\propto \omega^{-8}$ .

As shown in Fig. 2 (c), the influence of the mass on the transfer function is a simple rescaling as  $F(\omega)$  is proportional to  $m_0^{-2}$  according to Eqs. (8) and (9). Therefore, the phase fluctuation,  $\Gamma_{\text{noise}}$ , defined in Eq.(5) is independent of the mass  $m_0$ . This property suggests that when designing a matter-wave interferometer, one may choose the mass without the restriction from the noises.

### 3. GGN IN MATTER-WAVE INTERFEROMETERS

In this section, we will analyse the phase fluctuation density due to the GGN. In the Fermi normal coordinate system, constructed near the worldline of the laboratory [74], the Lagrangian in a non-relativistic limit is given by [37]

$$L_{\text{free-falling}} = \frac{1}{2} m_0 v^2 - m_0 a_0 x - \frac{1}{2} m_0 \underbrace{R_{0101} c^2}_{\equiv \omega_{gg}^2(t)} x^2, \quad (11)$$

where the superposition direction is defined along the  $x$ -axis as shown in Fig. 1. The first term on the right-hand side of Eq. (11) corresponds to a free-falling particle in a flat spacetime, and the other terms  $m_0 a_0 x$  and  $\frac{1}{2} m_0 R_{0101} c^2 x^2$  can be regarded as the acceleration noise and the GGN caused by fluctuations in the metric, respectively [37].

For a free-falling experiment, the acceleration term  $a_0$  will vanish according to the properties of the Fermi normal coordinates (in line with Einstein's equivalence principle), so this noise will be neglected in this paper. Therefore, we will solely focus on the noise  $\omega_{gg}^2(t)$  in Eq. (11), which corresponds to the noise  $\omega_{\text{noise}}^2$  in Sec. 2. As discussed, we characterize such a stochastic quantity by the noise PSD (see Eq. (4)). In particular, we introduce the GGN PSD  $S_{gg}(\omega)$  by the inverse-Fourier transformation, that is

$$S_{gg}(\omega) = \int \mathbb{E}[\omega_{gg}^2(t) \omega_{gg}^2(t + \tau)] e^{i\omega\tau} d\tau \\ \int \mathbb{E}[R_{0101}(t) R_{0101}(t + \tau)] c^4 e^{i\omega\tau} d\tau, \quad (12)$$

which has units of  $[\text{Hz}^4/\text{Hz}]^6$ .

There are many sources of GGN as noted in [57–60], but in this paper we will focus on one particular source of GGN due to the smooth motion of external objects. In the next section we first adapt the two-dimensional classical analysis from [69] to matter-wave interferometry in three-spatial dimensions.

### 4. THREE DIMENSIONAL GGN

To quantify the achievable sensitivity for measuring GGN in three spatial dimensions we first compute the corresponding PSD  $S_{gg}(\omega)$ . Consider the model shown in Fig. 3, and suppose that the external object whose

<sup>6</sup>  $S_{gg}(\omega) \sim \omega_{gg}^4/\omega$ , where  $\omega_{gg}$  describes the spacetime curvature noise and  $\omega$  is the Fourier transformation frequency, so we write the unit as  $[\text{Hz}^4/\text{Hz}]$  rather than  $[\text{Hz}^3]$ .

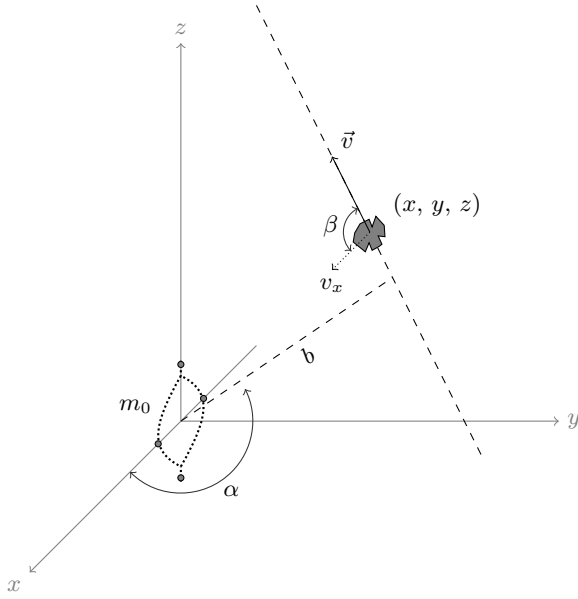


FIG. 3: Three-dimensional GGN caused by the smooth motion of an external object. The external object is located at a point  $(x, y, z)$  at time  $t$ , and moves with a constant velocity  $\vec{v} = (v_x, v_y, v_z)$ , while the interferometer of mass  $m_0$  is located at the origin, with the superposition along the  $x$ -axis. The impact parameter is denoted here as  $b$ , and the projection angles are defined as  $\cos \alpha = x_0/b$  and  $\cos \beta = v_x/v$ , where  $x_0$  is the  $x$ -coordinate at  $t = 0$  and  $v_x$  is the  $x$ -component of the constant velocity  $\vec{v}$ .

coordinate is denoted by  $\vec{r} = (x, y, z)$  moves with a uniform velocity  $\vec{v} = (v_x, v_y, v_z)$ , and with an impact parameter  $b$ . Then the local acceleration of the interferometer caused by the external mass at a given time,  $t$ , will be given by:

$$\begin{aligned} \vec{a}(t) &= \frac{GM}{r^2(t)} \frac{\vec{r}(t)}{r(t)} \\ &= \frac{GM}{r^3(t)} x(t) \vec{e}_x + \frac{GM}{r^3(t)} y(t) \vec{e}_y + \frac{GM}{r^3(t)} z(t) \vec{e}_z, \end{aligned} \quad (13)$$

where  $\vec{e}_j$  ( $j = x, y, z$ ) are the unit basis vectors. Since the external mass is assumed to be moving with a uniform velocity, one can write down  $r^2(t) = b^2 + v^2 t^2$  and  $x(t) = x_0 + v_x t$  if  $t = 0$  is defined as the time when the external object is at the closest point. Further, if we introduce the projection angles

$$\cos \alpha = x_0/b, \quad \cos \beta = v_x/v, \quad (14)$$

then the  $x$ -direction component of the acceleration  $\vec{a}$  can be written as

$$\begin{aligned} a_x(t) &= \frac{GM}{b^2} \frac{x_0/b + v_x t/b}{(1 + v^2 t^2/b^2)^{3/2}} \\ &= \frac{GM}{b^2} \frac{\cos \alpha + (vt/b) \cos \beta}{(1 + v^2 t^2/b^2)^{3/2}}. \end{aligned} \quad (15)$$

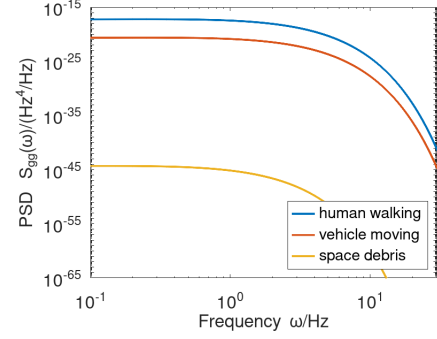


FIG. 4: The PSD of the GGN of several sources including human walking, vehicles moving and space debris according to Eq. (20). The masses are set as 50 kg,  $10^3$  kg and  $10^3$  kg in respect, the speeds are 1 m/s, 10 m/s and  $5 \times 10^4$  m/s respectively, and the impact parameter is set as 1 m, 10 m and  $10^5$  m in respect. As is discussed in the gravitational-wave literature [57, 61, 63], the GGN usually has a dominant contribution in low-frequency range. The PSD of GGN are usually smaller than  $10^{-20}$  Hz<sup>4</sup>/Hz [61, 63], while it can reach  $10^{-15}$  Hz<sup>4</sup>/Hz level for human walking, and this is the reason why ultra-sensitive experiments require an exclusion zone for human activities [37, 59, 69]. In this work, we however propose to detect such tiny GGN signals by designing a suitable interferometer, i.e., by optimizing the transfer function in Eq. (9). As we discuss in the text, by tuning the interferometric times we can obtain a transfer function which can induce a detectable phase fluctuation  $\Gamma_{gg}$  in specific frequency ranges.

Then in the frequency space, the Fourier transform of  $a_x(t)$  is given by <sup>7</sup>

$$\begin{aligned} a_x(\omega) &= \frac{GM}{b^2} \left( \frac{\omega b}{v} \right) \left[ \frac{x_0}{v} K_1 \left( \frac{\omega b}{v} \right) + i \frac{b v_x}{v} K_0 \left( \frac{\omega b}{v} \right) \right] \\ &= \frac{a_{\text{loc}}}{\omega} u_\omega^2 [\cos \alpha K_1(u_\omega) + i \cos \beta K_0(u_\omega)], \end{aligned} \quad (16)$$

where  $K_0(\cdot)$  and  $K_1(\cdot)$  are the modified Bessel functions. In the second line of Eq. (16) we have introduced the local acceleration,  $a_{\text{loc}}$ , and the frequency-dependent dimensionless ratio,  $u_\omega$ , defined as

$$a_{\text{loc}} \equiv GM/b^2, \quad u_\omega \equiv \omega b/v, \quad (17)$$

which, as we will see, control the behaviour of the GGN.

The PSD of the acceleration noise on  $a_x(\omega)$  can be

<sup>7</sup> Note that the superposition of the interferometer is along the  $x$ -axis and hence we project the acceleration vector along this direction.

computed as <sup>8</sup>

$$S_{aa}(\omega) = \frac{|a_x(\omega)|^2}{b/v}, \quad (18)$$

where  $b/v$  can be regarded as the scattering time between the external mass and the interferometer (in this context, playing the role of the signal and sensor, respectively). Combining Eqs. (16) and (18) one can obtain the PSD of the acceleration noise

$$S_{aa}(\omega) = \frac{a_{\text{loc}}^2}{\omega} u_\omega^3 [\cos^2 \alpha K_1^2(u_\omega) + \cos^2 \beta K_0^2(u_\omega)]. \quad (19)$$

Finally, the PSD of the GGN,  $S_{gg}(\omega) = S_{aa}(\omega)/b^2$ , is given by

$$S_{gg}(\omega) = \frac{a_{\text{loc}}^2}{\omega b^2} u_\omega^3 [\cos^2 \alpha K_1^2(u_\omega) + \cos^2 \beta K_0^2(u_\omega)]. \quad (20)$$

For example, the PSD of several sources such as human walking, vehicles moving, and space debris moving with a constant velocity is shown in Fig. 4. In gravitational-wave interferometers,  $S_{gg}(\omega)$  is regarded as a source of noise, and is mitigated from  $10^{-15}$  Hz<sup>4</sup>/Hz down to about  $10^{-20}$  Hz<sup>4</sup>/Hz for human walking by setting a suitable exclusion zones[37, 59, 61, 63, 69].

We want to devise an interferometer that is capable of detecting such weak GGN signals in the low-frequency range, by optimizing the interferometric parameters. From Eqs. (5) and (20) we find that the the corresponding phase fluctuation is given by

$$\Gamma_{gg} = \left( \frac{2m_0 a_{\text{loc}}}{\hbar b} \right)^2 \int \frac{u_\omega^3 F(\omega)}{\omega} [\cos^2 \alpha K_1^2(u_\omega) + \cos^2 \beta K_0^2(u_\omega)] d\omega. \quad (21)$$

In experiments the minimum measurable value of  $\Gamma_{gg}$  will be determined by the the overall phase sensitivity. In the following we will use  $\Gamma_{gg} = 0.01$  as the threshold value below which we can no longer reliable measure phase fluctuations. Given such a threshold value for  $\Gamma_{gg}$  we can then ask what should be the characteristic of the interferometer such that it can discern a particular GGN

signal. The interferometer mass  $m_0$  and the the superposition size  $\Delta x$  control the overall amplitude of the signal, while the beam-splitting time  $t_a$  and free-fall time  $t_e$  also control the sensitivity in a particular frequency range.

From Eq. (21) we can find the local gravitational acceleration

$$a_{\text{loc}}(M) = \frac{\hbar b \sqrt{\Gamma_{gg}}}{2m_0} \left( \int \frac{u_\omega^3 F(\omega)}{\omega} (\cos^2 \alpha K_1^2(u_\omega) + \cos^2 \beta K_0^2(u_\omega)) d\omega \right)^{-1/2}, \quad (22)$$

where the right-hand side fixes all the parameters, except the mass  $M$  of the external object. Eq. (22) thus provides a simple expression to estimate the minimum acceleration that one can sense given the threshold phase sensitivity  $\Gamma_{gg}$ . Since the impact parameter,  $b$  is also fixed on the right-hand side of Eq. (22) we find from Eq. (17) that the minimum detectable mass  $M$  of the external object with impact factor  $b$  (moving with velocity  $v$ , and with its direction parameterized by the angles  $\alpha$  and  $\beta$ ), is given by  $M = a_{\text{loc}} b^2 / G$ .

When  $\omega b/v \gg 1$  we can make some further approximations which are useful to investigate slow external objects (see Sec. 5.1). In this latter regime, the modified Bessel functions can be approximated as

$$K_0(u_\omega) \approx K_1(u_\omega) \approx \sqrt{\frac{\pi}{2}} \frac{e^{-u_\omega}}{\sqrt{u_\omega}}. \quad (23)$$

Then the GGN PSD in Eq. (20) can be reduced to:

$$S_{gg}(\omega) = \frac{a_{\text{loc}}^2}{\omega b^2} u_\omega^2 (\cos^2 \alpha + \cos^2 \beta) e^{-2u_\omega}. \quad (24)$$

Based on the reduced PSD in Eq. (24) the local acceleration Eq. (22) can be simplified to

$$a_{\text{loc}} = \frac{\hbar v}{2m_0} \sqrt{\frac{\Gamma_{gg}}{(\cos^2 \alpha + \cos^2 \beta) \int \omega F(\omega) e^{-2u_\omega} d\omega}}. \quad (25)$$

Physically, the condition  $\omega b/v \geq 1$  gives  $b/v \geq 1/\omega_{\text{min}} \sim t_{\text{exp}}$ , which constrains the interaction time,  $b/v$ , to be longer than the interferometric times,  $t_a, t_e$ . For example, a walking person moving with speed  $\sim 1$  m/s at a distance  $\sim 1$  m, so the corresponding ratio  $b/v \sim 1$  s satisfies the condition  $b/v \geq t_e, t_a \sim 1$  s. In Appendix A will show how the obtained three dimensional model reduces to the two dimensional result in [69] where the regime  $\omega b/v \geq 1$  has been assumed.

However, the approximation in Eq. (25) gives reasonable values as long as we are in the regime  $\tilde{\omega}_j b/v \gg 1$ , where  $\tilde{\omega}_j = 2\pi/t_j$  ( $j = a, e$ ) denotes the characteristic frequencies of the interferometer. The latter regime has the following hierarchy of times:

$$t_a, t_e \ll b/v \ll t_{\text{exp}}, \quad (26)$$

where we recall that  $t_{\text{exp}}$  is the total experimental time,  $b/v$  can be interpreted as the interaction time, and  $t_a, t_e$

<sup>8</sup> According to the Wiener-Khinchin theorem, the PSD of  $a_x(\omega)$  is given by  $S_{aa}(\omega) = \int \mathbb{E}[a(t)a(t+\tau)]e^{i\omega\tau} d\tau$ . The statistical average  $\mathbb{E}[a(t)a(t+\tau)]$  can be calculated by time average  $\mathbb{E}[a(t)a(t+\tau)] = \frac{1}{T} \int a(t)a(t+\tau)dt$ , where the time interval can be chosen as  $T = b/v$  in this model. Then one can obtain the formula of PSD as

$$\begin{aligned} S_{aa}(\omega) &= \frac{1}{T} \int \int a(t)a(t+\tau)e^{i\omega\tau} d\tau dt \\ &= \frac{1}{T} \int \int a(t_1)a(t_2)e^{i\omega(t_1-t_2)} dt_1 dt_2 \\ &= \frac{1}{T} \left| \int a(t)e^{i\omega t} dt \right|^2 = \frac{|a_x(\omega)|^2}{b/v}. \end{aligned}$$

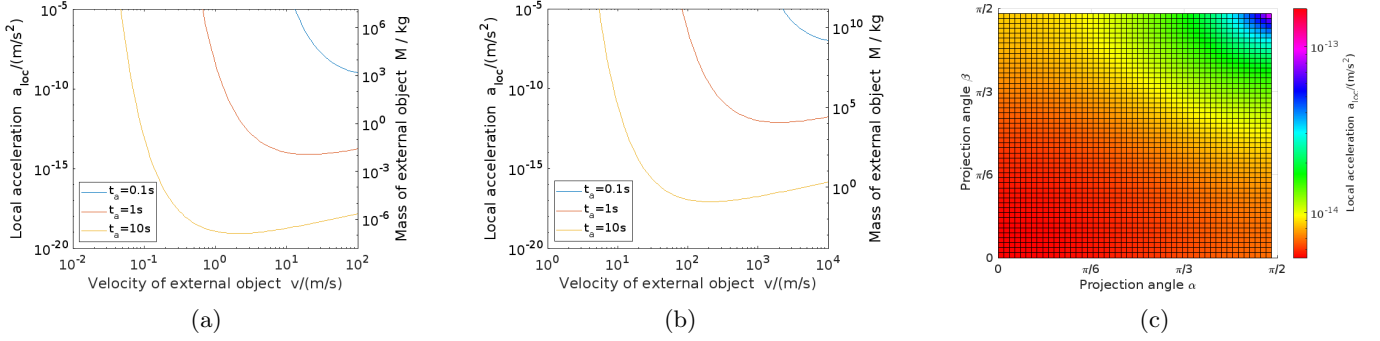


FIG. 5: (a) The left-most panel shows the Plot of minimum detectable local acceleration  $a_{loc} = GM/b$  (left vertical-axis), or equivalently, the minimum detectable mass of the GGN source (right vertical-axis). The GGN source has an impact parameter  $b = 10$  m and velocity  $v$  (horizontal-axis). The GGN sensitivity increases by increasing the beam-splitting time  $t_a$  (the free-falling time  $t_e = 0$  s for simplicity such that the total interferometric time is  $4t_a$ . The beam-splitting acceleration  $a_m$  is set as  $1.8 \times 10^{-2}$  m/s<sup>2</sup> (the corresponding magnetic field gradient is  $\nabla B = 10^4$  T/m) and the mass of the interferometer is  $m_0 = 10^{-17}$  kg. (b) The middle panel shows similar to (a) but with the impact parameter set to  $b = 1000$  m, requiring longer beam-splitting times  $t_a$  to achieve the same sensitivity for the minimum detectable mass (corresponding to a better sensitivity of the minimum detectable local acceleration). (c) The right most panel shows the colour map for the minimum detectable local acceleration as a function of the projection angles  $\alpha$  (horizontal-axis) and  $\beta$  (vertical-axis) quantifying the relative orientation of the interferometer and the motion of the external object (see Fig. 3). The impact factor has been set to  $b = 10$  m and the velocity to  $v = 10$  m/s. The optimal sensitivity is achieved when the motion of the external object is aligned with the axis of the interferometer ( $\alpha = 0$  and  $\beta = 0$ ).

are the beam-splitting time and free-evolution time of a single interferometric loop, respectively. In such a regime we can make the approximation  $F(\omega) \approx \bar{F}$ , where  $\bar{F}$  is defined in Eq. (10). The integrations in Eq. (22) then reduce to

$$\int_0^\infty u_\omega^2 K_0^2(u_\omega) du_\omega = \frac{\pi^2}{32} \approx 0.31, \quad (27)$$

$$\int_0^\infty u_\omega^2 K_1^2(u_\omega) du_\omega = \frac{3\pi^2}{32} \approx 0.93, \quad (28)$$

where we have changed the integration variable to  $u_\omega = b\omega/v$  defined in Eq. (17). On the other hand, using the approximation in Eq. (23), the relevant integration in Eq. (22) evaluates to:

$$\int_0^\infty u_\omega \left( \sqrt{\frac{\pi}{2}} \frac{e^{-u_\omega}}{\sqrt{u_\omega}} \right)^2 du_\omega = \frac{\pi}{8} \approx 0.40. \quad (29)$$

which is of the same order of magnitude as the results obtained in Eqs. (27) and (28). Since in this work we are primarily interested in the order of magnitude estimates, we will thus use the approximation in Eq. (25) also for the regime given in Eq. (26) (see Sec. 5.2 below).

## 5. SENSING GGN

We now apply the model developed in the previous sections to sense GGN from three different types of sources. For simplicity we will set the free-fall time to  $t_e = 0$  and vary only the beam-splitting time  $t_a$ . We will first focus on sensing GGN in the vicinity of Earth-based laboratories and sensing space-debris in the vicinity of satellites

(Sec. 5.1). The goal of these two sections is to check the feasibility of tracking the motion of the objects, ideally in real-time, and hence we consider the total experimental time to be the smallest possible, i.e.,  $t_{\text{exp}} = 4t_a$ . To make a statistically significant number of experimental runs we would thus need to consider an array of interferometers operating simultaneously. We will conclude with an order of magnitude estimate about the requirements for detecting the motion of heavy dim objects in the outer solar system (Sec. 5.2). In this latter section we are not so much interested in real-time tracking but rather in ascertaining the existence of a tiny signal. Hence we will consider the experimental time to be infinite, i.e., we will work in the limit  $t_{\text{exp}} \rightarrow \infty$  to maximize the GGN signal. In this case one needs to perform a large number of experimental runs either using a single interferometer or an array of interferometers.

### 5.1. GGN sources in Earth-based laboratories and space-debris in the vicinity of satellites

In this section, we quantify the sensitivity to GGN signals caused by the motion of small objects in the proximity of experiments. As we will see, unknown light objects, even if moving at slow speeds, can be a significant source of GGN for state-of-the-art experiments, which become sensitive to tiny local accelerations.

We first focus on GGN sources that could be present inside Earth-based laboratories. In particular, we will consider external objects in the velocity range ( $10^{-2}$  –  $10^2$ ) m/s, and with masses in the range from ( $10^{-5}$  –  $10^3$ ) kg. We will further assume that the external object,

acting as the GGN source, has an impact factor  $b = 10$  m.

As discussed in Sec. 4 we will set the GGN phase to the value  $\Gamma_{gg} \geq 0.01$ <sup>9</sup>. If one fixes also the beam-splitting time  $t_a$  one can then evaluate the local acceleration  $a_{loc}$ . Using Eq. (17) one can then readily determine also the minimum detectable mass  $M$  of the GGN source. To remain in the regime  $b\omega/v \gg 1$ , where we can use the simple formula in Eq. (25), we will consider only beam-splitting times smaller than  $t_a \sim 10$  s.

As shown in Fig. 5 (a), when  $v \rightarrow 0$  or  $v \rightarrow \infty$ , the local acceleration  $a_{loc}$  tends to infinity and the minimum detectable mass  $M$  becomes extremely large. Indeed, when the external object moves too slowly or too fast, its GGN signal decreases as the frequency range of the interferometer  $\sim t_a^{-1}$  is no longer compatible with the characteristic frequency of the GGN source given by  $v/b$ . The interferometer performs optimally as a GGN sensor when  $t_a^{-1}$  is comparable to  $b/v$ .

A similar analysis as discussed above can be also adapted for sensing space debris in the vicinity of satellites [75, 76]. For illustration, we will consider the debris at impact factor  $b = 1000$  m and with velocity in the range  $(10^0 - 10^4)$  m/s. We consider the same beam-splitting times as in the previous section, although the beam-splitting time could be significantly extended in space [77, 78]. In Fig. 5 (b) we show the measurable local acceleration, or equivalently, the minimum detectable mass of the GGN source.

In Fig. 5 (c) we also show the minimum detectable mass as a function of the projection,  $\cos \alpha$  and  $\cos \beta$ , defined in Eq. (14) evaluated for a fixed beam-splitting time  $t_a$ , fixed velocity  $v = 10$  m/s, and fixed impact factor  $b = 10$  m. The optimal sensitivity is achieved for  $\cos \alpha = \cos \beta = 1$  corresponding the external object moving along the  $x$ -axis.

## 5.2. Primordial Black Hole in the Outer Solar System and Rogue Asteroids

It has recently been suggested to look for primordial black holes in the outer solar systems using a dedicated space mission [79]. Such objects are not a sources of light (apart from the tiny Hawking radiation) and hence one can only infer their motion from nearby object's (such as stars or planets) paths which themselves will be very dim (as they are far away any significant light source). As such, the existence of a primordial black hole in the outer solar system is yet to be ascertained by any means.

While such heavy outer solar system objects are invisible for optical/radio astronomy they cannot conceal its

motion from a GGN gravitational detector (albeit their GGN signature is far beyond current interferometers as we will see). Here we estimate the interferometric requirements to sense their GGN signature limiting the discussion to an order of magnitude estimate using Eq. (25). We suppose we are in the regime of Eq. (26) and further assume  $\cos^2 \alpha + \cos^2 \beta \sim 1$ . Furthermore, as discussed in Sec. 2 the transfer function at low frequencies can be taken to be approximately constant,  $F(\omega) \approx \bar{F}$ , such that the integration in Eq. (25) can be carried out to obtain<sup>10</sup>

$$a_{loc} \sim \frac{\hbar b \sqrt{\Gamma_{gg}}}{m_0 \sqrt{\bar{F}}}. \quad (30)$$

Using the definition of the local acceleration in Eq. (17) we hence find from Eq. (25):

$$\bar{F} = 2\Delta x^4 t_a^2 \sim \frac{\hbar^2 b^6}{G m_0 M} \Gamma_{gg}, \quad (31)$$

where the first equality is the expression for the asymptotic low frequency transfer function defined in Eq. (10).

For the outer solar primordial black hole we consider the following values [80–83]: impact factor  $b = 500$  a.u.  $\approx 10^{14}$  m and mass  $M = 10^{25}$  kg, while the velocity does not affect the result (the velocity of the external mass cancelled out in the lowest order term in Eq. (31)). Setting the mass of the interferometer to  $m_0 \sim 1$  g we find from Eq. (31) that a superposition size  $\Delta x \sim 10$  cm and the beam-splitting time  $t_a \sim 1$  s would be sufficient to measure an outer solar black hole for  $\Gamma_{gg} \sim 0.01$ . Such numbers are however beyond the reach of foreseeable interferometric experiments in the near future.

In a similar vein, we can discuss the GGN arising from a rogue asteroid hitting earth [84]. For example, consider an asteroid of mass  $M \sim 10^7$  kg (similar to the Tunguska event in 1908) hurling towards Earth. Such an object could be detected at a distance of  $b \sim 10^{11}$  m (roughly a hundred times the Earth-Moon distance) using again an interferometer of mass  $m_0 \sim 1$  g, superposition size  $\Delta x \sim 10$  cm, and beam-splitting time  $t_a \sim 1$  s. Although such massive interferometers are way beyond our current reach, there are discussions on creating a mass independent scheme for realising large superpositions [48, 49].

For comparison we can compare the size of the GGN caused by Earth. Here we are considering the sensor to be falling towards the Earth – in the co-moving reference frame of the sensor, the center of the Earth moves

<sup>10</sup> We use that

$$\int_{\omega_{\min}}^{\infty} \omega F(\omega) e^{-2b\omega/v} d\omega \approx \frac{\bar{F}(v^2 + 2v\omega_{\min})}{4b^2} e^{-2b\omega_{\min}/v} \approx \frac{\bar{F}v^2}{4b^2},$$

where  $\bar{F}$  is the value of  $F(\omega)$  at low frequencies. In the last equality we have assumed, as a crude approximation, that we can take the limit  $\omega_{\min} \rightarrow 0$  such that the integration simplifies to  $v^2/(4b^2)$ , i.e. we assume that the available experimental time is infinite.

<sup>9</sup> In a concrete experiment one has estimate the achievable phase sensitivity by characterizing various background noises. Here the value  $\Gamma_{gg} \geq 0.01$  is chosen as a concrete example (see comment below Eq. (21)).



towards the sensor with the impact parameter as the radius of the Earth  $b \sim 6400$  km. Using again (31) we find that an interferometer of mass  $m_0 \sim 1$  g would be sensitive to the Earth's GGN using a superposition size  $\Delta x \sim 10$  fm and the beam-splitting time  $t_a \sim 1$  s.

## 6. SUMMARY

We first made a brief review of frequency-space analysis for matter-wave interferometry. We pointed out that the spectral density of the phase fluctuation caused by a noise can be always factorized into the noise part (described by the corresponding PSD) and the trajectory part (described by the so-called transfer function defined by Eq. (6)). An interesting observation is that the transfer function of the configuration shown in Fig. 1 is proportional to the square of the mass of the interferometer, and hence according to Eq. (5) the phase fluctuation  $\Gamma_{\text{noise}}$  no longer depends on it (i.e, the factors  $\propto m_0^2$  in the numerator and denominator cancel out exactly). While we have primarily focused on a SG scheme with nanoparticles, the latter observation suggests that a similar analysis could be readily adapted to other types of matter-wave interferometers, such as those based on ultra-cold atom Bose-Einstein Condensate (BEC)[2, 3, 5, 85, 86].

We have developed a 3D model for the GGN signal of a moving external object, and obtained the corresponding PSD in Eq. (20), generalizing the two dimensional model in [69]. Based on the PSD of gravity gradient signal, we then derived the expression Eq. (22) and Eq. (25) which quantifies the local gravitational acceleration, or equivalently, the minimum detectable mass of the GGN source.

Finally, we applied the developed model to investigate two distinct GGN sources, namely, slow moving objects in Earth-based laboratories and space debris near satellites, and studied how the GGN signal varies with the velocity, distance, and orientation. We concluded by estimating the requirements to sense weak GGN signals caused by object in the outer solar system and rogue asteroids.

Of course, there are numerous challenges to be met before we can realize experimentally such a quantum sensor. Creating large spatial superpositions and achieving the required coherence time with large masses is a formidable challenge. Nonetheless, we foresee that a nanoparticle matter-wave interferometer can have many novel technological applications, complementing the fundamental tests of Newton's law or detecting the quantum gravity induced entanglement.

## Acknowledgments

We would like to thank Ryan Marshman for helpful discussions. M. Wu would like to thank the China Scholarship Council (CSC) for financial support. MT

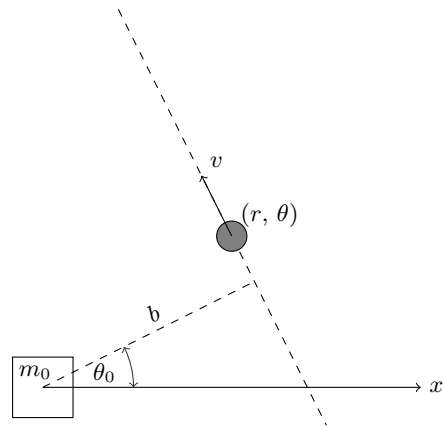


FIG. 6: The two dimensional model for GGN caused by a smooth motion. The external object is originally located at point  $(b, \theta_0)$ , and moves with a constant speed  $v$ .

acknowledges funding by the Leverhulme Trust (RPG-2020-197). SB would like to acknowledge EPSRC grants No. EP/N031105/1 and EP/S000267/1.

## Appendix A: GGN in two dimensions

In this appendix, we will show how the 3D model developed in Sec. 3 reduces to a two-dimensional model when the external object and the quantum sensor are confined to a plane (see Fig. 6). Comparing to the 3D model from the main text, we only need one polar angle  $\theta$  to describe the motion of the external object moving at impact factor  $b$ . As we will see below, if we further set the angle to  $\theta_0 = 0$ , then the two dimensional model reduces to the original model proposed in [69].

The acceleration caused by the Newtonian force in the  $x$ -direction is given by:

$$a_x(t) = \frac{GM}{b^2} \frac{1}{(1 + (vt/b)^2)^{3/2}} (\cos \theta_0 + (vt/b) \sin \theta_0), \quad (\text{A1})$$

so in the frequency space, the local acceleration is

$$a_x(\omega) = \frac{GM}{b^2 \omega} u_\omega^2 (\cos \theta_0 K_1(u_\omega) + i \sin \theta_0 K_0(u_\omega)), \quad (\text{A2})$$

where  $K_\alpha(\cdot)$  is the modified Bessel function, and we have introduced  $u_\omega = b\omega/v$  (see Eq. (17) in the main text). Comparing to the three dimensional result in Eq. (16), the projection angle  $\alpha$  and  $\beta$  becomes  $\theta_0$  and  $\pi/2 - \theta_0$ , respectively.

According to  $S_{aa}(\omega) = |a_x(\omega)|^2/(b/v)$  and  $S_{gg}(\omega) = S_{aa}(\omega)/b^2$ , the GGN PSD in the two dimensional case is given by:

$$S_{gg}(\omega) = \frac{a_{\text{loc}}^2 u_\omega^3}{\omega b^2} [\cos^2 \theta_0 K_1^2(u_\omega) + \sin^2 \theta_0 K_0^2(u_\omega)], \quad (\text{A3})$$

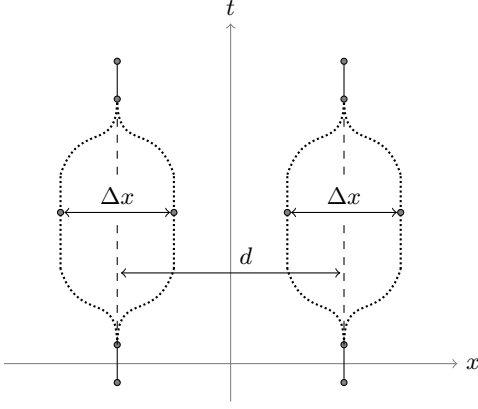


FIG. 7: Illustration of the paths of the dual interferometer. A single symmetric interferometer is by itself not susceptible to a GGN signal as one can always choose the origin of the coordinate system, corresponding to the origin of the harmonic GGN metric perturbation, such that the paths are located symmetrically on each side (for example, the paths of the right interferometer are symmetric with respect to  $x = d/2$  and the phases on each arm would become proportional to  $\propto (\pm\Delta x/2)^2$  – one only generates an undetectable global phase on an individual interferometer). However, if one is considering joint observables of multiple interferometers placed along the  $x$ -axis, one can no longer make the phases on an individual interferometer  $\propto x^2$  equal, leading to a nonzero GGN signal. Indeed, in the picture the phases on the two arms of the left (right) interferometer are given by  $\propto (-d/2 \pm \Delta x/2)^2$  ( $\propto (d/2 \pm \Delta x/2)^2$ ). More generally, two or more adjacent symmetric interferometers can become sensitive to GGN when the two arms of an individual individual interferometer are placed asymmetrically with respect to the origin of the local GGN metric perturbation [37].  $d$  is the distance between the two interferometers, and  $\Delta x$  is the superposition size, assumed equal for both interferometers.

where we have introduced  $a_{\text{loc}} = GM/b^2$  (see Eq. (17) in the main text). The corresponding phase fluctuation is

$$\Gamma_{gg} = \left( \frac{2m_0 a_{\text{loc}}}{\hbar b} \right)^2 \int \frac{u_\omega^3 F(\omega)}{\omega} [\cos^2 \theta_0 K_1^2(u_\omega) + \sin^2 \theta_0 K_0^2(u_\omega)] d\omega. \quad (\text{A4})$$

From Eq. (A4) we then readily find the local acceleration:

$$a_{\text{loc}}(M) = \frac{\hbar b \sqrt{\Gamma_{gg}}}{2m_0} \left( \int \frac{u_\omega^3 F(\omega)}{\omega} (\cos^2 \theta_0 K_1^2(u_\omega) + \sin^2 \theta_0 K_0^2(u_\omega)) d\omega \right)^{-1/2}. \quad (\text{A5})$$

If we now set  $\theta_0 = 0$  we recover the result presented in [69]. In the regime  $u_\omega \gg 1$  the modified Bessel's function can be approximated as  $K_0(u_\omega) \sim K_1(u_\omega) \sim e^{-u_\omega}/u_\omega^{1/2}$  (see Eq. (23) in the main text). In this regime the GGN PSD in Eq. (A3) reduces to

$$S_{gg}(\omega) = \frac{a_{\text{loc}}^2}{b^2 \omega} u_\omega^2 e^{-2\omega b/v}. \quad (\text{A6})$$

The GGN formula Eq. (A6) remains a decent approximation even when  $u_\omega \sim 1$  which is the regime considered in [69] where they have omitted the dimensionless prefactor  $u_\omega^2$ . Finally, using Eq. (A6) we find that the local acceleration simplifies to the simple expression:

$$a_{\text{loc}} = \frac{\hbar v}{2m_0} \sqrt{\frac{\Gamma_{gg}}{\int \omega F(\omega) e^{-2u_\omega} d\omega}}, \quad (\text{A7})$$

which matches Eq. (25) for  $\alpha = 0$  and  $\beta = \pi/2$ .

## Appendix B: GGN with two symmetric interferometers

For completeness we discuss the dual QGEM interferometer depicted in Fig. 7. Each individual interferometer (the left one or the right one) has the paths located asymmetrically with respect to the origin – as such, the two paths of an individual interferometer acquire a nonzero phase difference from the harmonic trap generated by a GGN signal centered at the origin. In case, one is looking at joint properties of the two interferometers, such as an entanglement witness, the dual interferometer becomes sensitive to GGN [37].

The transfer function for symmetric interferometer is given by [37]:

$$F(\omega) = 64d^2 a_m^2 \frac{\sin^4(\frac{\omega t_a}{2}) \sin^2(\frac{1}{2}\omega(2t_a + t_e))}{\omega^6}. \quad (\text{B1})$$

where  $d$  denotes the distance between the centers of two interferometers (the rest of the parameters have the same meaning to the ones defined in the main text). We discuss the minimum local acceleration (or equivalently, the minimum detectable mass) from GGN signals in Fig. 8. We note that the dual QGEM interferometer is less sensitive to GGN signals in comparison to the asymmetric MIMAC interferometer.

[1] Kai Bongs and Klaus Sengstock. Physics with coherent matter waves. *Reports on Progress in Physics*, 67(6):907–963, may 2004.

[2] Chris Overstreet, Peter Asenbaum, Tim Kovachy, Remy Notermans, Jason M. Hogan, and Mark A. Kasevich. Effective inertial frame in an atom interferometric test of

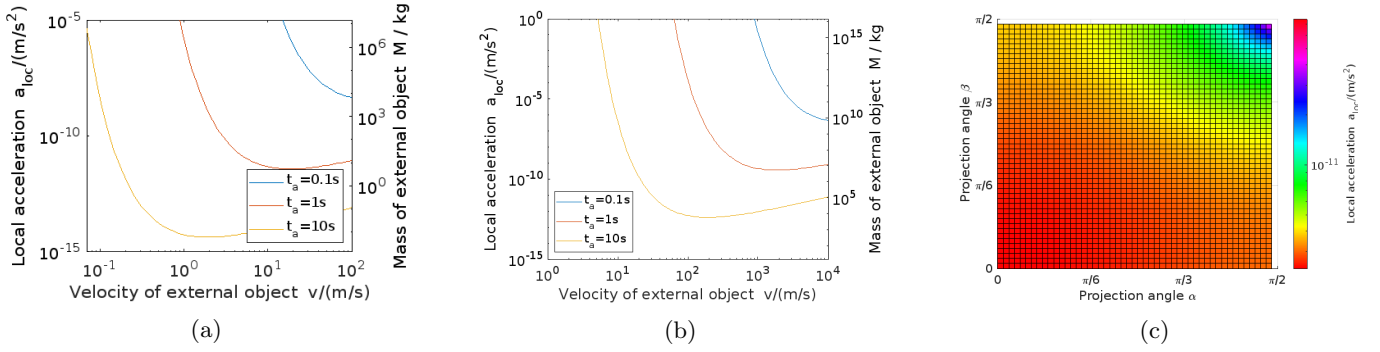


FIG. 8: Same as Fig. 5 but for the dual interferometer in Fig. 7 with the transfer function given in Eq. (B1). The mass of an individual interferometer is  $m_0 = 10^{-17}$  kg, and we have set the distance between the two interferometers to  $d = 100$  m and the beam-splitting acceleration  $a_m = 1.8 \times 10^{-2}$  m/s<sup>2</sup> corresponding to the magnetic field gradient  $\nabla B = 10^4$  T/m. (a) Plot of minimum detectable local acceleration, or equivalently, of the minimum detectable mass of the GGN source. The impact factor is set to  $b = 10$  m. (b) Same as (a) but with the impact parameter set to  $b = 1000$  m. (c) Colour map for the minimum detectable local acceleration as a function of the projection angles  $\alpha$  and  $\beta$ . The impact factor of the external object has been set to  $b = 10$  m and the velocity to  $v = 10$  m/s.

- the equivalence principle. *Phys. Rev. Lett.*, 120:183604, May 2018.
- [3] Peter Asenbaum, Chris Overstreet, Minjeong Kim, Joseph Curti, and Mark A. Kasevich. Atom-interferometric test of the equivalence principle at the  $10^{-12}$  level. *Phys. Rev. Lett.*, 125:191101, Nov 2020.
- [4] Sougato Bose, Anupam Mazumdar, Martine Schut, and Marko Toroš. Entanglement Witness for the Weak Equivalence Principle. 3 2022.
- [5] Achim Peters, Keng Yeow Chung, and Steven Chu. Measurement of gravitational acceleration by dropping atoms. *Nature*, 400(6747):849–852, Aug 1999.
- [6] Ryan J. Marshman, Anupam Mazumdar, Gavin W. Morley, Peter F. Barker, Steven Hoekstra, and Sougato Bose. Mesoscopic Interference for Metric and Curvature (MI-MAC) & Gravitational Wave Detection. *New J. Phys.*, 22(8):083012, 2020.
- [7] Raymond Y. Chiao and Achilles D. Speliotopoulos. Towards MIGO, the Matter wave Interferometric Gravitational wave Observatory, and the intersection of quantum mechanics with general relativity. *J. Mod. Opt.*, 51:861, 2004.
- [8] Albert Roura, Dieter R. Brill, B. L. Hu, and Charles W. Misner. Gravitational wave detectors based on matter wave interferometers (MIGO) are no better than laser interferometers (LIGO). *Phys. Rev. D*, 73:084018, 2006.
- [9] Stefano Foffa, Alice Gasparini, Michele Papucci, and Riccardo Sturani. Sensitivity of a small matter-wave interferometer to gravitational waves. *Phys. Rev. D*, 73:022001, 2006.
- [10] Savas Dimopoulos, Peter W. Graham, Jason M. Hogan, Mark A. Kasevich, and Surjeet Rajendran. An Atomic Gravitational Wave Interferometric Sensor (AGIS). *Phys. Rev. D*, 78:122002, 2008.
- [11] Savas Dimopoulos, Peter W. Graham, Jason M. Hogan, Mark A. Kasevich, and Surjeet Rajendran. Gravitational Wave Detection with Atom Interferometry. *Phys. Lett. B*, 678:37–40, 2009.
- [12] Guglielmo M. Tino et al. SAGE: A Proposal for a Space Atomic Gravity Explorer. *Eur. Phys. J. D*, 73(11):228, 2019.
- [13] Peter Asenbaum, Chris Overstreet, Minjeong Kim, Joseph Curti, and Mark A. Kasevich. Atom-Interferometric Test of the Equivalence Principle at the  $10^{-12}$  Level. *Phys. Rev. Lett.*, 125(19):191101, 2020.
- [14] Peter W. Graham, Jason M. Hogan, Mark A. Kasevich, and Surjeet Rajendran. A New Method for Gravitational Wave Detection with Atomic Sensors. *Phys. Rev. Lett.*, 110:171102, 2013.
- [15] R. Colella, A. W. Overhauser, and S. A. Werner. Observation of gravitationally induced quantum interference. *Phys. Rev. Lett.*, 34:1472–1474, Jun 1975.
- [16] SA Werner, J-L Staudenmann, and R Colella. Effect of earth’s rotation on the quantum mechanical phase of the neutron. *Physical Review Letters*, 42(17):1103, 1979.
- [17] Helmut Rauch and Samuel A. Werner. *Neutron Interferometry: Lessons in Experimental Quantum Mechanics, Wave-Particle Duality, and Entanglement*. Oxford University Press, 01 2015.
- [18] Valery V. Nesvizhevsky, Hans G. Börner, Alexander K. Petukhov, Hartmut Abele, Stefan Baeßler, Frank J. Rueß, Thilo Stöferle, Alexander Westphal, Alexei M. Gagarski, Guennady A. Petrov, and Alexander V. Strelkov. Quantum states of neutrons in the earth’s gravitational field. *Nature*, 415(6869):297–299, Jan 2002.
- [19] J. B. Fixler, G. T. Foster, J. M. McGuirk, and M. A. Kasevich. Atom interferometer measurement of the newtonian constant of gravity. *Science*, 315(5808):74–77, 2007.
- [20] Peter Asenbaum, Chris Overstreet, Tim Kovachy, Daniel D Brown, Jason M Hogan, and Mark A Kasevich. Phase shift in an atom interferometer due to spacetime curvature across its wave function. *Physical review letters*, 118(18):183602, 2017.
- [21] Chris Overstreet, Peter Asenbaum, Joseph Curti, Minjeong Kim, and Mark A Kasevich. Observation of a gravitational aharonov-bohm effect. *Science*, 375(6577):226–229, 2022.
- [22] G Bertocchi, O Alibart, D B Ostrowsky, S Tanzilli, and P Baldi. Single-photon sagnac interferometer. *Journal of Physics B: Atomic, Molecular and Optical Physics*, 39(5):1011–1016, feb 2006.
- [23] Matthias Fink, Ana Rodriguez-Aramendia, Johannes

- Handsteiner, Abdul Ziarkash, Fabian Steinlechner, Thomas Scheidl, Ivette Fuentes, Jacques Pienaar, Timothy C. Ralph, and Rupert Ursin. Experimental test of photonic entanglement in accelerated reference frames. *Nature Communications*, 8(1):15304, May 2017.
- [24] Sara Restuccia, Marko Toroš, Graham M. Gibson, Hendrik Ulbricht, Daniele Faccio, and Miles J. Padgett. Photon bunching in a rotating reference frame. *Phys. Rev. Lett.*, 123:110401, Sep 2019.
- [25] Marko Toroš, Sara Restuccia, Graham M Gibson, Marion Cromb, Hendrik Ulbricht, Miles Padgett, and Daniele Faccio. Revealing and concealing entanglement with non-inertial motion. *Physical Review A*, 101(4):043837, 2020.
- [26] Marion Cromb, Sara Restuccia, Graham M Gibson, Marko Toroš, Miles J Padgett, and Daniele Faccio. Controlling photon entanglement with mechanical rotation. *arXiv preprint arXiv:2210.05628*, 2022.
- [27] Marko Toroš, Marion Cromb, Mauro Paternostro, and Daniele Faccio. Generation of entanglement from mechanical rotation. *arXiv preprint arXiv:2207.14371*, 2022.
- [28] Sougato Bose, Anupam Mazumdar, Gavin W. Morley, Hendrik Ulbricht, Marko Toroš, Mauro Paternostro, Andrew A. Geraci, Peter F. Barker, M. S. Kim, and Gerard Milburn. Spin entanglement witness for quantum gravity. *Phys. Rev. Lett.*, 119:240401, Dec 2017.
- [29] [https://www.youtube.com/watch?v=0Fv-0k13s\\_k](https://www.youtube.com/watch?v=0Fv-0k13s_k), 2016. Accessed 1/11/22.
- [30] C. Marletto and V. Vedral. Gravitationally induced entanglement between two massive particles is sufficient evidence of quantum effects in gravity. *Phys. Rev. Lett.*, 119:240402, Dec 2017.
- [31] Ryan J. Marshman, Anupam Mazumdar, and Sougato Bose. Locality and entanglement in table-top testing of the quantum nature of linearized gravity. *Phys. Rev. A*, 101(5):052110, 2020.
- [32] Sougato Bose, Anupam Mazumdar, Martine Schut, and Marko Toroš. Mechanism for the quantum natured gravitons to entangle masses. *Phys. Rev. D*, 105(10):106028, 2022.
- [33] Marios Christodoulou, Andrea Di Biagio, Markus Aspelmeyer, Časlav Brukner, Carlo Rovelli, and Richard Howl. Locally mediated entanglement through gravity from first principles. 2 2022.
- [34] Daine L. Danielson, Gautam Satishchandran, and Robert M. Wald. Gravitationally mediated entanglement: Newtonian field versus gravitons. *Phys. Rev. D*, 105(8):086001, 2022.
- [35] H Pino, J Prat-Camps, K Sinha, B Prasanna Venkatesh, and O Romero-Isart. On-chip quantum interference of a superconducting microsphere. *Quantum Science and Technology*, 3(2):025001, jan 2018.
- [36] Thomas W. van de Kamp, Ryan J. Marshman, Sougato Bose, and Anupam Mazumdar. Quantum gravity witness via entanglement of masses: Casimir screening. *Phys. Rev. A*, 102:062807, Dec 2020.
- [37] Marko Toroš, Thomas W. Van De Kamp, Ryan J. Marshman, M. S. Kim, Anupam Mazumdar, and Sougato Bose. Relative acceleration noise mitigation for nanocrystal matter-wave interferometry: Applications to entangling masses via quantum gravity. *Phys. Rev. Res.*, 3(2):023178, 2021.
- [38] Jules Tilly, Ryan J. Marshman, Anupam Mazumdar, and Sougato Bose. Qudits for witnessing quantum-gravity-induced entanglement of masses under decoherence. *Phys. Rev. A*, 104(5):052416, 2021.
- [39] Martine Schut, Jules Tilly, Ryan J. Marshman, Sougato Bose, and Anupam Mazumdar. Improving resilience of quantum-gravity-induced entanglement of masses to decoherence using three superpositions. *Phys. Rev. A*, 105(3):032411, 2022.
- [40] H. Chau Nguyen and Fabian Bernards. Entanglement dynamics of two mesoscopic objects with gravitational interaction. *The European Physical Journal D*, 74(4):69, Apr 2020.
- [41] Hadrien Chevalier, A. J. Paige, and M. S. Kim. Witnessing the nonclassical nature of gravity in the presence of unknown interactions. *Phys. Rev. A*, 102:022428, Aug 2020.
- [42] B. Friedrich and H. Schmidt-Böcking. *Molecular Beams in Physics and Chemistry: From Otto Stern's Pioneering Exploits to Present-Day Feats*. Springer International Publishing, 2021.
- [43] Mark Keil, Shimon Machluf, Yair Margalit, Zhifan Zhou, Omer Amit, Or Dobkowski, Yonathan Japha, Samuel Moukouri, Daniel Rohrllich, Zina Binstock, Yaniv Bar-Haim, Menachem Givon, David Groswasser, Yigal Meir, and Ron Folman. *Stern-Gerlach Interferometry with the Atom Chip*, pages 263–301. Springer International Publishing, Cham, 2021.
- [44] Shimon Machluf, Yonathan Japha, and Ron Folman. Coherent stern-gerlach momentum splitting on an atom chip. *Nature Communications*, 4(1):2424, Sep 2013.
- [45] Yair Margalit, Or Dobkowski, Zhifan Zhou, Omer Amit, Yonathan Japha, Samuel Moukouri, Daniel Rohrllich, Anupam Mazumdar, Sougato Bose, Carsten Henkel, and Ron Folman. Realization of a complete stern-gerlach interferometer: Toward a test of quantum gravity. *Science Advances*, 7(22):eabg2879, 2021.
- [46] Ryan J. Marshman, Anupam Mazumdar, Ron Folman, and Sougato Bose. Constructing nano-object quantum superpositions with a Stern-Gerlach interferometer. *Phys. Rev. Res.*, 4(2):023087, 2022.
- [47] Run Zhou, Ryan J. Marshman, Sougato Bose, and Anupam Mazumdar. Catapulting towards massive and large spatial quantum superposition. 6 2022.
- [48] Run Zhou, Ryan J. Marshman, Sougato Bose, and Anupam Mazumdar. Mass Independent Scheme for Large Spatial Quantum Superpositions. 10 2022.
- [49] Run Zhou, Ryan J. Marshman, Sougato Bose, and Anupam Mazumdar. Gravito-diamagnetic forces for mass independent large spatial quantum superpositions. 11 2022.
- [50] Berthold-Georg Englert, Julian Schwinger, and Marlan O. Scully. Is spin coherence like humpty-dumpty? i. simplified treatment. *Foundations of Physics*, 18(10):1045–1056, Oct 1988.
- [51] J. Schwinger, M. O. Scully, and B.-G. Englert. Is spin coherence like humpty-dumpty? *Zeitschrift für Physik D Atoms, Molecules and Clusters*, 10(2):135–144, Jun 1988.
- [52] MO Scully, BG Englert, and J Schwinger. Spin coherence and humpty-dumpty. iii. the effects of observation. *Physical review. A, General physics*, 40(4):1775—1784, August 1989.
- [53] Yonathan Japha and Ron Folman. Role of rotations in Stern-Gerlach interferometry with massive objects. 2 2022.
- [54] Massimo Inguscio. Majorana "spin-flip" and ultra-low temperature atomic physics. *PoS*, EMC2006:008, 2007.

- [55] Marko Toroš, Anupam Mazumdar, and Sougato Bose. Loss of coherence of matter-wave interferometer from fluctuating graviton bath. *arXiv preprint arXiv:2008.08609*, 2020.
- [56] Fabian Gunnink, Anupam Mazumdar, Martine Schut, and Marko Toroš. Gravitational decoherence by the apparatus in the quantum-gravity induced entanglement of masses. 10 2022.
- [57] Jan Harms. Terrestrial gravity fluctuations. *Living Reviews in Relativity*, 22(1):6, Oct 2019.
- [58] Scott A. Hughes and Kip S. Thorne. Seismic gravity-gradient noise in interferometric gravitational-wave detectors. *Phys. Rev. D*, 58:122002, Nov 1998.
- [59] Kip S. Thorne and Carolee J. Winstein. Human gravity-gradient noise in interferometric gravitational-wave detectors. *Phys. Rev. D*, 60:082001, Sep 1999.
- [60] M. Beccaria et al. Relevance of Newtonian seismic noise for the VIRGO interferometer sensitivity. *Class. Quant. Grav.*, 15:3339–3362, 1998.
- [61] et.al. F. Acernese. Advanced virgo: a second-generation interferometric gravitational wave detector. *Classical and Quantum Gravity*, 32(2):024001, dec 2014.
- [62] T. Akutsu, M. Ando, Sakae Araki, Akito Araya, T. Arima, N. Aritomi, H. Asada, Yoichi Aso, S. Atsuta, K. Awai, Luca Baiotti, M. Barton, Dan Chen, Kyuman Cho, K. Craig, Riccardo Desalvo, K. Doi, K. Eda, Y. Enomoto, and A. Yanagida. Construction of kagra: an underground gravitational wave observatory. 11 2017.
- [63] Maria Bader, Soumen Koley, Jo van den Brand, Xander Campman, Henk Jan Bulten, Frank Linde, and Bjorn Vink. Newtonian-noise characterization at terziet in limburg—the euregio meuse–rhine candidate site for einstein telescope. *Classical and Quantum Gravity*, 39(2):025009, jan 2022.
- [64] John M. Goodkind. The superconducting gravimeter. *Review of Scientific Instruments*, 70(11):4131–4152, 1999.
- [65] Ryan J Marshman, Anupam Mazumdar, Gavin W Morley, Peter F Barker, Steven Hoekstra, and Sougato Bose. Mesoscopic interference for metric and curvature and gravitational wave detection. *New Journal of Physics*, 22(8):083012, aug 2020.
- [66] Sofia Qvarfort, Alessio Serafini, P. F. Barker, and Sougato Bose. Gravimetry through non-linear optomechanics. *Nature Communications*, 9(1):3690, Sep 2018.
- [67] F. Armata, L. Latmiral, A. D. K. Plato, and M. S. Kim. Quantum limits to gravity estimation with optomechanics. *Phys. Rev. A*, 96:043824, Oct 2017.
- [68] Markus Rademacher, James Millen, and Ying Lia Li. Quantum sensing with nanoparticles for gravimetry: when bigger is better. *Advanced Optical Technologies*, 9(5):227–239, 2020.
- [69] Peter R. Saulson. Terrestrial gravitational noise on a gravitational wave antenna. *Phys. Rev. D*, 30:732–736, Aug 1984.
- [70] Pippa Storey and Claude Cohen-Tannoudji. The feynman path integral approach to atomic interferometry. a tutorial. *Journal de Physique II*, 4(11):1999–2027, 1994.
- [71] Vinay Ingle, Stephen Kogon, and Dimitris Manolakis. *Statistical and adaptive signal processing*. Artech, 2005.
- [72] Chris Chatfield. *The analysis of time series: an introduction*. Chapman and hall/CRC, 2003.
- [73] Graham P. Greve, Chengyi Luo, Baochen Wu, and James K. Thompson. Entanglement-enhanced matter-wave interferometry in a high-finesse cavity. *Nature*, 610(7932):472–477, Oct 2022.
- [74] Eric Poisson, Adam Pound, and Ian Vega. The motion of point particles in curved spacetime. *Living Reviews in Relativity*, 14(1):7, Sep 2011.
- [75] Gurudas Ganguli, Chris Crabtree, Leonid Rudakov, and Scott Chappie. A concept for elimination of small orbital debris. *TRANSACTIONS OF THE JAPAN SOCIETY FOR AERONAUTICAL AND SPACE SCIENCES, AEROSPACE TECHNOLOGY JAPAN*, 10, 04 2011.
- [76] Heather Mae Cowardin, J. c. Liou, P. Krisko, John N. Opiela, Norman G. Fitz-Coy, Marlon E. Sorge, and T. Huynh. Characterization of orbital debris via hypervelocity laboratory-based tests. 2017.
- [77] David C Aveline, Jason R Williams, Ethan R Elliott, Chelsea Dutenhoffer, James R Kellogg, James M Kohel, Norman E Lay, Kamal Oudrhiri, Robert F Shotwell, Nan Yu, et al. Observation of bose–einstein condensates in an earth-orbiting research lab. *Nature*, 582(7811):193–197, 2020.
- [78] Giulio Gasbarri, Alessio Belenchia, Matteo Carlesso, Sandro Donadi, Angelo Bassi, Rainer Kaltenbaek, Mauro Paternostro, and Hendrik Ulbricht. Testing the foundation of quantum physics in space via interferometric and non-interferometric experiments with mesoscopic nanoparticles. *Communications Physics*, 4(1):1–13, 2021.
- [79] Edward Witten. Searching for a black hole in the outer solar system. *arXiv preprint arXiv:2004.14192*, 2020.
- [80] Chadwick A. Trujillo and Scott S. Sheppard. A Sedna-like body with a perihelion of 80 astronomical units. *Nature*, 507(7493):471–474, March 2014.
- [81] Konstantin Batygin and Michael E. Brown. Evidence for a Distant Giant Planet in the Solar System. *APJ*, 151(2):22, February 2016.
- [82] Konstantin Batygin, Fred C. Adams, Michael E. Brown, and Juliette C. Becker. The planet nine hypothesis. *Physics Rept.*, 805:1–53, May 2019.
- [83] Jakub Scholtz and James Unwin. What if Planet 9 is a Primordial Black Hole? *Phys. Rev. Lett.*, 125(5):051103, 2020.
- [84] Clemens M. Rumpf, Hugh G. Lewis, and Peter M. Atkinson. Asteroid impact effects and their immediate hazards for human populations. *Geophysical Research letters*, 44(8):3433–3440, April 2017.
- [85] Chris Overstreet, Peter Asenbaum, Joseph Curti, Minjeong Kim, and Mark A. Kasevich. Observation of a gravitational aharonov-bohm effect. *Science*, 375(6577):226–229, 2022.
- [86] Albert Roura. Quantum probe of space-time curvature. *Science*, 375(6577):142–143, 2022.